

Fabrication and photocatalytic property of ZnSe nanosheets

JIAJIA YIN, GUOYING FENG*, SHOUHUAN ZHOU*

Institute of Laser & Micro/Nano Engineering, College of Electronics & Information Engineering, Sichuan University, Chengdu Sichuan, 610065, China

ZnSe nanosheets have been fabricated by femtosecond laser ablation in distilled water at room temperature. Their crystal structure, crystal phase, shape and size distribution, and photophysical property are investigated using X-ray diffraction (XRD), Raman spectroscopy, field emission scanning electron microscopy (FE-SEM), transmission electron microscopy (TEM), high resolution transmission electron microscopy (HRTEM) and UV-Vis spectroscopy. The as-prepared ZnSe nanosheets efficiently catalyze the photodegradation of methyl orange (MO) present in aqueous solutions under visible light irradiation, exhibiting higher photocatalytic activity than ZnSe microsized particles. The high photoactivity of the nanosheets can be attributed to the combined effects of large surface areas and the more unsaturated surface coordination sites exposed to the solution.

(Received March 28, 2015; accepted May 7, 2015)

Keywords: Femtosecond laser ablation, ZnSe nanosheets, Photodegradation

1. Introduction

In recent years, ZnSe has attracted huge attention as an important Zn-based compound. It's a direct band gap semiconductor with a room-temperature bulk bandgap of 2.67 eV [1,2,3]. The optoelectronic properties of ZnSe is exceptional so that ZnSe has a wide range of applications, such as light-emitting diodes, blue-ultraviolet photodetector, biomedical sensors, piezoelectric nanogenerator, and photo-voltaic solar cells, et al. [4,5,6,7,8,9]. In particular, the photocatalytic activity of ZnSe makes it a promising catalytic material in photocatalytic degradation of organic pollutants. In the studies of ZnSe, many researches about the "Nanostructuring" of it have been reported. Because of the higher surface-to-volume ratios and higher redox-potentials with the increase of band gap energy caused by "quantum size effect", "Nanostructuring" of the photolytic materials is identified as one of the most promise ways to gain factorial enhancements in photocatalysts. According to the previous studies, different types of ZnSe such as nanoparticles [10,11], nanorods [12,13] and thin films [14], flowerlike hierarchical structure [15] have been developed for studying their photocatalytic characteristics [8,9]. Hence the technology of preparing different types of nanosubstructured ZnSe photocatalysts doubtless deserves to be taken into account in future research.

In recent years, laser ablation in liquid mediums has been widely used in the synthesis of nanocrystals and fabrication of nanostructures due to the following

advantages: (i) being performed in a controllable contamination-free environment this method makes possible the production of nanomaterials without impurities [16,17,18,19], and (ii) the high pressure and high temperature environment condition created by laser ablation in liquids is fast, moderate, and safe, excluding the potential of explosion [20,21,22]. (iii) the property of the synthesized nanoparticles (e.g. shape, size, distribution, etc.) can be conveniently controlled upon laser ablation in liquids by changing laser parameters and kinds of solutions [23,24,25,26,27,28,29,30]. Furthermore, compared with other normal laser ablation, femtosecond laser ablation has some advantages, such as higher temperature and higher pressure in a local volume can be achieved, higher temperature phase materials can be fabricated, and smaller nanocrystals with narrow size distribution can be obtained [17,19].

In this work, we present a facile method of femtosecond pulsed laser ablation in liquid mediums (FPLAL) for the synthesis of ZnSe nanosheets. The ZnSe nanosheets photocatalyst shows a better photocatalytic activity in comparison with the microsized powder before FPLAL under visible light.

2. Experimental section

2.1 Synthesis of ZnSe nanosheets

All chemicals were of analytical grade and used as

received without further purification. A typical experimental setup of pulsed laser ablation in liquid was shown in Fig. 1. First, the femtosecond laser was produced by a regenerative amplified mode-locked Ti:sapphire laser (Coherent Inc., 35 fs in duration and 1 kHz repetition rate) operating at a wavelength of 800 nm. Next, the targets, microsized ZnSe particles with 99.999% purity, for laser ablation were prepared by standard mechanical grinding method. Sufficient powder was put into the vessel, and distilled water was poured slowly into the vessel about 10 mm. Finally, the pulsed laser was focused via a lens onto the water-suspended ZnSe microsized particles, and the solution was continuously stirred with a magnetic stirrer during laser irradiation. After FPLAL, the suspensions were ultrasonically dispersed for 30 min and left at rest in a temperature-controlled bath having a constant temperature of 50 °C.

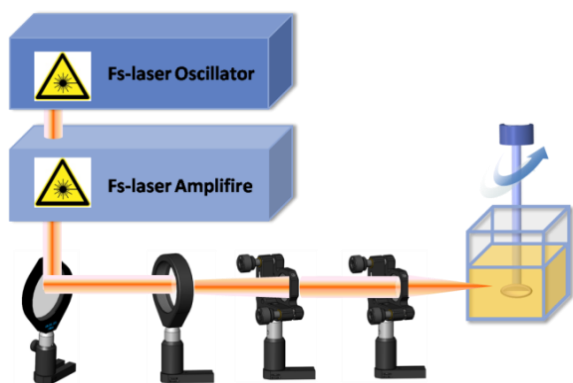


Fig. 1. Typical experimental setup for laser ablation in liquids.

2.2 Photocatalytic experiments

Photocatalytic experiments in aqueous solution were performed in a water-cooled quartz vessel. The visible light was generated from a 300 W Xe lamp. A suspension containing ZnSe nanosheets catalysts (30 mg) and methyl orange (MO) aqueous solution (30 mL, 5.0×10^{-5} M) was magnetically stirred in the dark for 60 min to establish an adsorption/desorption equilibrium of the dye species. At given irradiation time intervals (1 h), a series of aqueous solutions in a certain volume (2ml) were collected and centrifugation for analysis. The distance between the light source and the bottom of the solution was about 10 cm. The concentrations of MO were monitored by using a UV-Vis spectrometer.

2.3 Characterization of the samples

X-ray powder diffraction (XRD) patterns were recorded on a Japan Rigaku D/max-rB X-ray diffractometer with Cu K α radiation ($\lambda=0.154178$ nm), operated at 40 kV and 80 mA. A Raman spectrum (Renishaw, RM 1000) was recorded by using excitation

from the 633 nm line of a He-Ne laser. Field-emission scanning electron microscopy (FESEM) measurements were carried out on a field-emission microscope (Hitachi SU-8220) operated at an acceleration voltage of 3 kV. Transmission electron microscopy (TEM) images were taken with a Hitachi H-800 transmission electron microscope, operated at an acceleration voltage of 200 kV. The variation of the methyl orange concentration was evaluated by the photoluminescence intensity, which was determined by a Hitachi F-4500 fluorescence spectrophotometer.

3. Results and discussion

3.1 Morphology and structure

The morphology and size of the as-synthesized products were characterized by FESEM. Fig. 2(a) is picture of the ZnSe microsized particles prepared by standard mechanical grinding method. As shown in Fig. 2(b), after the FPLAL process only nanoparticles were generated. The transmission electron microscopy image (Fig. 1(b')) reveals that nanoparticles with an average size of 10 nm have been created in aqueous environment by using 800 nm radiation with 1 mJ femtosecond pulsed laser. After the suspensions were ultrasonically dispersed and seted a period of time, nucleation and growth of ZnSe Nanosheets occurs at the solid–liquid interface. The yield of hierarchical nanostructures is high. Fig. 2(c) and (d) show the FESEM image of the nanosheets.

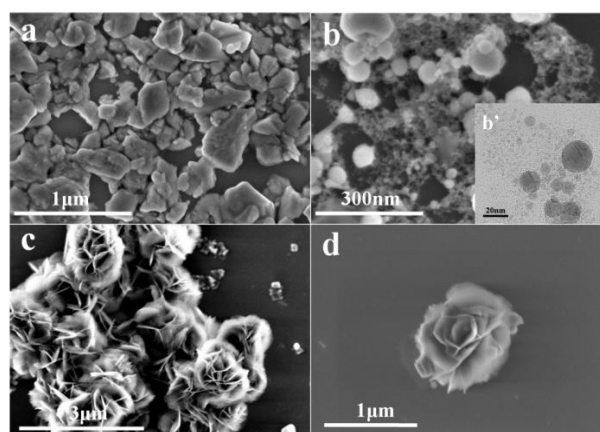


Fig. 2. SEM images of (a) ZnSe microsized particles prepared by standard mechanical grinding method; (b) ZnSe nanoparticles prepared by FPLAL; (c) and (d) are ZnSe nanosheets.

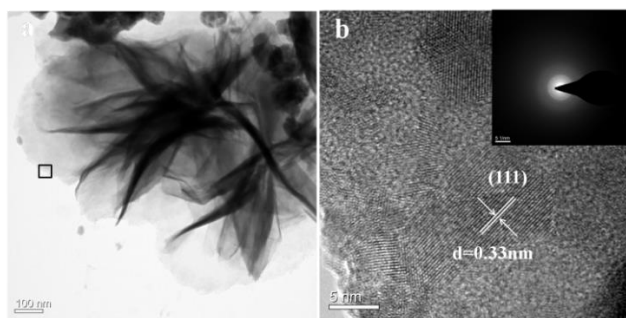


Fig. 3. (a)TEM image, (b)HRTEM images of ZnSe nanosheets. The inset of (b) is the electron diffraction image.

Further insight into the morphology and nanostructure of ZnSe nanosheets was gained by using TEM and high-resolution TEM (HRTEM). Fig. 3(a) shows the low-magnification TEM image of a single ZnSe nanosheets with diameters of 0.5-1 μ m. Fig. 3(b) shows a typical HRTEM image of a single nanosheet which indicates that the sheet is polycrystalline consisting of single-crystalline grains with characteristic size of about 10 nm and random orientation. The inset of Fig. 3(b) is the corresponding selected area electron diffraction (SAED) pattern. The lattice fringes ($d=0.33$ nm) observed in the HRTEM image agree well with the separation between the (111) lattice planes.

It's interesting to investigate growth process of nanosheets because in the FPLAL process only nanoparticles were prepared, as shown in Fig. 2(b). The liquid surface has a large accommodation coefficient so that prepared nanoparticles has preferred depositions in the suspension. Interaction forces between atoms in prepared nanoparticles result in nanoparticles' translation and rotation movements, which driving them to find appropriate locations and orientations for aggregation. Then growth of ZnSe nanosheets occurs at the solid-liquid interface since the liquid becomes super-saturated with nanoparticles.

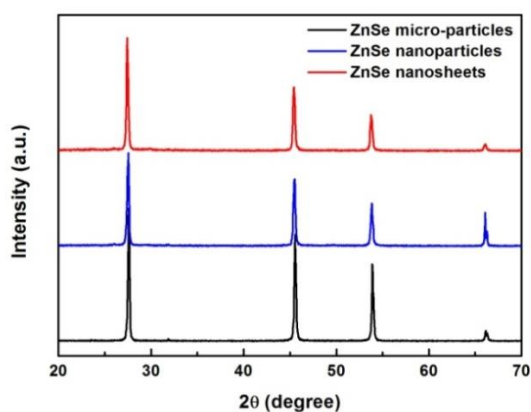


Fig. 4. X-ray diffraction patterns of ZnSe micro-sized particles, ZnSe nanoparticles, and ZnSe nanosheets.

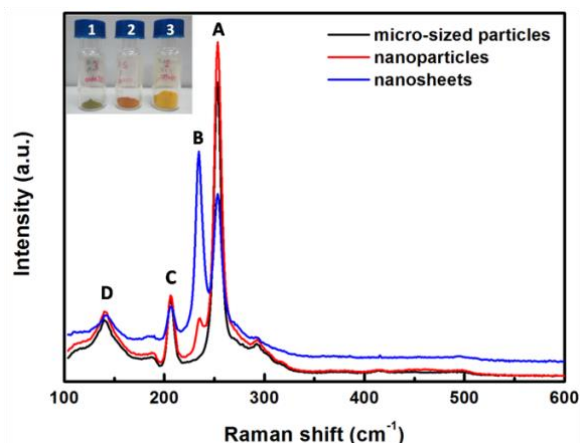


Fig. 5. Room-temperature Raman spectrum of (a)ZnSe micro-sized particles ,(b)ZnSe nanoparticles,(c)ZnSe nanosheets.

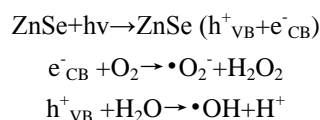
The phases and purities of the as-prepared samples were investigated by the XRD analysis. Fig. 4 shows the XRD pattern of the samples. The three patterns all fits well with face-centered cubic (fcc) ZnSe with lattice constants $a=5.668$ Å (JCPDS 37-1463). No other diffraction peaks can be found in the pattern, indicating no impurity was present in the as-synthesized samples.

It has been demonstrated that Raman spectroscopy is a fast and nondestructive tool for assessing crystalline material quality, including surface conditions and homogeneity [31]. Hence, the structure characterization of the as-prepared ZnSe nanosheets is further studied via Raman measurement by using the 633 nm excitation line at room temperature which is shown in Fig. 5. The Raman spectrum exhibits peaks at 253.4, 234.6, 205.9, and 139.9 cm^{-1} are labeled A, B, C, and D, respectively. According to the reported study [32,33,34], peak A is assigned to the longitudinal optical (LO) phonon scattering of the ZnSe crystal. Peaks C and D, which could be assigned to 2TA, TO, respectively [35, 36]. Peak B, at 234.6 cm^{-1} , between the TO and LO phonons, is thought to be the surface mode, for its position is very close to the value in previous literature (237 cm^{-1}) [37]. The appearance of surface phonons is a characteristic feature of small-size nanostructures [38]. As shown in Fig. 5, all three samples exhibit similar peak positions, but for the surface mode peak, the sample of ZnSe micro-sized particles doesn't exist. While the enhanced emission intensity of the ZnSe nanosheets indicates the more generated defects of the ZnSe nanosheets compared with the nanoparticles. The sharp Raman peak of sample 1 suggests that the ZnSe nanosheets are all of high crystalline quality and pure phase, which has been demonstrated by XRD analysis [34]. The inset on the right-top corner of Fig. 5 shows the photo of ZnSe nanosheets, ZnSe nanoparticles, and pure ZnSe micro-sized particles are labeled 1, 2 and 3.

3.2 Photocatalysts

Organic dyes are used extensively to color products in the textile industry, such as nylon, wool, cotton, and silk, as well as for coloring oil, fats, waxes, varnish, and plastics. Many dyes are nontoxic themselves at the concentration discharged into the receiving waters. However, they can easily form highly toxic complexes with some heavy metal ions (i.e., Cr, Al, and Cu) in wastewater to pollute water resource [39,40]. Methylene orange is the representation of aryl methane basic dyes, because the structure contains two benzene rings, being non-biodegradable, it is too stable to be decomposed easily by traditional chemical and biological treatment.

The photocatalytic activity of ZnSe nanosheets is evaluated in terms of the degradation of methyl orange (MO) dye in aqueous solution (5×10^{-5} M) under visible light irradiation or various durations at room temperature (Fig. 6(b)). For comparison, pure ZnSe microsized particles, and ZnSe nanoparticles were chosen as the reference photocatalysts. Fig. 6 shows the photodegradation results of MO catalyzed by all the catalysts. The characteristic absorption of MO at $\lambda=462$ nm is selected as monitoring the photocatalytic degradation process. The control analyses show that the degradation of MO is negligible without visible irradiation or in the absence of catalysts. It can be seen that the degradation efficiency by ZnSe microsized particles was low owing to less-defect crystal structure. On the contrary, the ZnSe nanosheets show a strong adsorptive capacity and comparable photocatalytic activity, which is much better than micro-size ZnSe and ZnSe nanoparticles. The decolor stages are shown in the inset of Fig. 6(a, b), from which it is clear that the orange color of the starting solution gradually disappears with increasing irradiation time, and the maximum absorbance disappears almost completely after irradiation for about 7h. The loss of absorbance may be due to the destruction of the dye chromogen. Referring to the previous papers [41,42,43,44,45,46], a possible mechanism of the photocatalytic activity for the degradation of methyl orange is proposed. $\bullet O_2$ and $\bullet OH$ present extremely strong oxidizing properties and are able to degrade the MO dye.



Under visible light irradiation, the pseudo-first-order constants for the photodegradation of MO are 0.218 h^{-1} (i.e., $3.63 \times 10^{-3} \text{ min}^{-1}$) and 0.089 h^{-1} (i.e., $1.48 \times 10^{-3} \text{ min}^{-1}$) with ZnSenanosheets or ZnSemicrosized particles, respectively (Fig. 6(c)). The linear relationship between $\ln(C_0/C)$ and time t can be achieved for the selected photodegradation curves of ZnSe nanosheets, ZnSe nanoparticles and ZnSe microsized particles (Fig. 6(d)).

And the degradation rate of ZnSe nanosheets is about twice that of ZnSe microsized particles. The high specific surface area and surface defects (the surface defects can absorb oxygen species (such as O_2^- , OH^-) that could change into high-activity $\text{O}_2^{\bullet-}$ and OH^\bullet , which can improve the photocatalysis reaction [47]) results in more unsaturated surface coordination sites exposed to the solution.

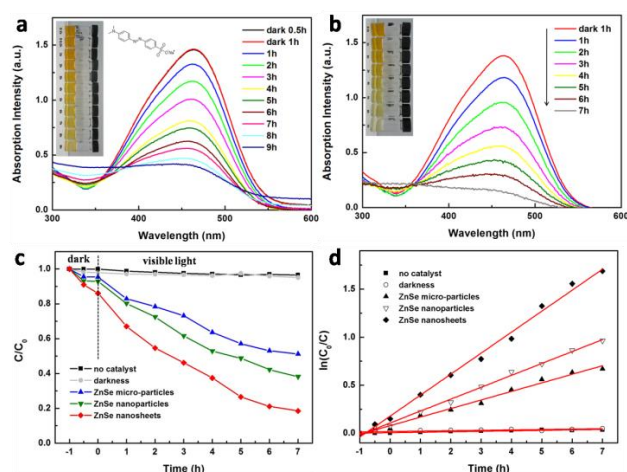


Fig. 6. Absorption spectrum of the MO solution and color changes (inset a, b) in the presence of ZnSe microsized particles(a) and ZnSe nanosheets (b) under the irradiation of the visible light for various durations. (c) Photodegradation curves of MO in water under visible light in the presence of catalysts (ZnSe microsized particles, ZnSe nanoparticles, ZnSenanosheets), without adding any catalyst, and in darkness in the presence of ZnSe nanosheets. (d) The selected fitting results using the pseudo-first-order reaction.

4. Conclusion

In summary, nanocrystalline ZnSe nanosheets have been successfully synthesized by femtosecond laser ablation in distilled water at room temperature. The as-synthesized ZnSe nanosheets are highly dispersed and uniform in size, the average size of ZnSe nanosheets is $1.2 \mu\text{m}$ and the thickness of a single ZnSe nanosheet is quite thin. The as-prepared ZnSe nanomaterials have also been demonstrated to work as effective photocatalysts and exhibit excellent photocatalytic activity for the degradation of methyl orange, which were found in different industries' effluents. The degradation rate of ZnSe nanosheets is about twice that of ZnSe microsized particles, suggesting that the as-synthesized ZnSe nanosheets are a more powerful photocatalyst for the degradation of MO dye. We demonstrated that sheet-like morphology was important for the excellent photocatalytic activity. A combination of their unique features of high surface to volume ratios,

monodispersion, easy recycling, and high photocatalytic activity may render these ZnSe nanosheets more practical applications, such as in semiconductor photocatalysis and environmental remediation.

Acknowledgement

We wish to thank Professor Zhengdong Cheng of Texas A&M University for useful discussions and help. This research is supported by Major Program of the National Natural Science Foundation of China (NSFC)(No. 60890200) and NSFC (No. 10976017).

References

- [1] S. Xiong, J. Shen, Q. Xie, Y. Gao, Q. Tang, Y. T. Qian, *Advanced Functional Materials* **15**(11), 1787 (2005).
- [2] B. Xiang, H. Z. Zhang, G. H. Li, F. H. Yang, F. H. Su, R. M. Wang, J. Xu, G. W. Lu, X. C. Sun, Q. Zhao, D. P. Yu, *Applied Physics Letters*, **82**(19), 3330 (2003).
- [3] C. R. Wang, J. Wang, Q. Li, G. C. Yi, *Advanced Functional Materials*, **15**(9), 1471 (2005).
- [4] C. C. Kim, S. Sivananthan, *Physical Review B* **53**(3), 1475 (1996).
- [5] H. Yu, J. Li, R. A. Loomis, P. C. Gibbons, W. E. Wang Buhro, *Journal of the American Chemical Society*, **125**(52), 16168 (2003).
- [6] Y.-W. Jun, J.-E. Koo, J. Cheon, *Chemical Communications*, (14), 1243 (2000).
- [7] H. I. Heulings, X. Huang, J. Li, T. Yuen, C. Lin, *Nano Letters*, **1**(10), 521 (2001).
- [8] H. Fujiwara, H. Hosokawa, K. Murakoshi, Y. Wada, S. Yanagida, T. Okada, H. Kobayashi, *The Journal of Physical Chemistry B*, **101**(41), 8270 (1997).
- [9] C. Liu, W. Zhang, J. Sun, J. Wen, Q. Yang, H. Cuo, X. Ma, M. Zhang, *Applied Surface Science*, **322**, 95 (2014).
- [10] X. Ma, Y. Shen, G. Wu, Q. Wu, B. Pei, M. Cao, F. Gu, *Journal of Alloys and Compounds*, **538**(0), 61 (2012).
- [11] M.-B. Saab, E. Estephan, T. Cloitre, C. Larroque, C. Gergely, *The Journal of Physical Chemistry C*, **114**(43), 18509 (2010).
- [12] J. Archana, M. Navaneethan, S. Ponnusamy, Y. Hayakawa, C. Muthamizhchelvan, *Materials Letters*, **64**(19), 2094 (2010).
- [13] G. Feng, C. Yang, S. Zhou, *Nano letters*, **13**(1), 272 (2013).
- [14] Y. G. Gudage, N. G. Deshpande, A. A. Sagade, R. Sharma, *Journal of Alloys and Compounds*, **488**(1), 157 (2009).
- [15] Y. Zhang, C. Hu, B. Feng, X. Wang, B. Wan, *Applied Surface Science*, **257**(24), 10679 (2011).
- [16] B. N. Chichkov, C. Momma, S. Nolte, von F. Alvensleben, A. Tünnermann, *Applied Physics A*, **63**(2), 109 (1996).
- [17] G. W. Yang, *Progress in Materials Science* **52**(4), 648 (2007).
- [18] L. Liao, Q. Zhang, Z. Su, Z. Zhao, Y. Wang, Y. Li, X. Lu, D. Wei, G. Feng, Q. Yu, *Nature nanotechnology*, **9**(1), 69 (2014).
- [19] V. Amendola, M. Meneghetti, *Physical chemistry chemical physics*, **11**(20), 3805 (2009).
- [20] F. Mafuné, J.-y. Kohno, Y. Takeda, T. Kondow, H. Abe, *The Journal of Physical Chemistry B*, **104**(39), 9111 (2000).
- [21] K. V. Anikin, N. N. Melnik, A. V. Simakin, G. A. Shafeev, V. V. Voronov, A. G. Vitukhnovsky, *Chemical Physics Letters*, **366**(3–4), 357 (2002).
- [22] G. Compagnini, A. A. Scalisi, O. Puglisi, *Physical Chemistry Chemical Physics*, **4**(12), 2787 (2002).
- [23] D. Beena, K. J. Lethy, R. Vinodkumar, A. P. Detty, V. P. Vahadevan Pillai, V. Ganesan, *Journal of Alloys and Compounds*, **489**(1), 215 (2010).
- [24] K. Praveena, K. Sadhana, S. R. Murthy, *Journal of Alloys and Compounds*, **492**(1–2), 245 (2010).
- [25] D. S. Milovanović, B. B. Radak, B. M. Gaković, D. Batani, M. D. Momčilović, M. S. Trtica, *Journal of Alloys and Compounds*, **501**(1), 89 (2010).
- [26] L. Yang, P. W. May, L. Yin, T. B. Scott, *Nanotechnology*, **18** (21), 215602 (2007).
- [27] T. Asahi, T. Sugiyama, H. Masuhara, *Accounts of Chemical Research*, **41**(12), 1790 (2008).
- [28] H. Cui, P. Liu, G. W. Yang, *Applied Physics Letters*, **89**(15), (2006).
- [29] P. Liu, Y. L. Cao, H. Cui, X. Y. Chen, G. W. Yang, *Chemistry of Materials*, **20**(2), 494 (2007).
- [30] P. Liu, Y. Cao, C. Wang, X. Chen, G. Yang, *Nano letters*, **8**(8), 2570 (2008).
- [31] H. Cao, G. Wang, J. H. Warner, A. A. R. Watt, *Applied Physics Letters*, **92**(1), (2008).
- [32] S. V. Pol, V. G. Pol, J. M. Calderon-Moreno, S. Cheylan, A. Gedanken, *Langmuir*, **24**(18), 10462 (2008).
- [33] Z. D. Hu, X. F. Duan, M. Gao, Q. Chen, L. M. Peng, *The Journal of Physical Chemistry C*, **111**(7), 2987 (2007).
- [34] L. Shi, Y. Xu, Q. Li, *The Journal of Physical Chemistry C*, **113**(5), 1795 (2009).
- [35] S. Anand, P. Verma, K. P. Jain, S. C. Abbi, *Physica B: Condensed Matter*, **226** (4), 331 (1996).
- [36] O. Pagès, M. A. Renucci, O. Briot, R. L. Aulombard, *Journal of Applied Physics*, **77**(3), 1241 (1995).
- [37] P. V. Teredesai, F. L. Deepak, A. Govindaraj, A. K. Sood, C. N. R. Rao, *Journal of Nanoscience and Nanotechnology*, **2**(5), 495 (2002).
- [38] Q. Xiong, J. Wang, O. Reese, L. C. Lew Yan Voon, P. C. Eklund, *Nano Letters*, **4**(10), 1991 (2004).
- [39] L. Zhang, H. Yang, J. Yu, F. Shao, L. Li, F. Zhang,

- H. Zhao, *The Journal of Physical Chemistry C*, **113**(14), 5434 (2009).
- [40] N. Kislov, J. Lahiri, H. Verma, D. Y. Goswami, E. Stefanakos, M. Batzill, *Langmuir*, **25**(5), 3310
- [41] W. Z. Tang, C. P. Huang, *Water Research*, **29**(2), 745 (1995).
- [42] S. K. Kansal, M. Singh, D. Sud, *Journal of Hazardous Materials*, **141** (3), 581 (2007).
- [43] X. Di, S. K. Kansal, W. Deng, *Separation and Purification Technology*, **68** (1), 61 (2009).
- [44] M. Sun, D. Li, W. Li, Y. Chen, Z. Chen, Y. He, X. Fu, *The Journal of Physical Chemistry C*, **112**(46), 18076 (2008).
- [45] C. Kormann, D. W. Bahnemann, M. R. Hoffmann, *Environmental Science & Technology*, **22**(7), 798 (1988).
- [46] A. J. Hoffman, E. R. Carraway, M. R. Hoffmann, *Environmental Science & Technology*, **28**(5), 776 (1994).
- [47] H.-M. Xiong, D. G. Shchukin, H. Möhwald, Y. Xu, Y.-Y. Xia, *Angewandte Chemie International Edition*, **48**(15), 2727 (2009).

*Corresponding author: guoing_feng@scu.edu.cn;
zhoush@scu.edu.cn